Inorganic Chemistry

pubs.acs.org/IC

Article

Gram-Scale, One-Pot Synthesis of a Cofacial Porphyrin Bridged by Ortho-xylene as a Scaffold for Dinuclear Architectures

Daoyang Zhang, Rachel L. Snider, Matthew R. Crawley, Ming Fang, Karla R. Sanchez-Lievanos, Spencer Ang, and Timothy R. Cook*

Cite This: *Inorg. Chem.* 2024, 63, 22532−22541

Read Online

ACCESS | Metrics & More | Article Recommendations | Supporting Information

ABSTRACT: Herein, we report the reaction between four 1,2-dibromoxylenes and two tetra-3-pyridylporphyrins for the formation of a cofacial porphyrin core spanned by dipyridinium xylene moieties. The metal-free organic nanocage (oNC) was synthesized in one twenty-four h step at a gram-scale with a 91.5% yield. The **free base oNC** was subsequently metalated with cobalt(II) (**Co-oNC**), copper(II) (**Cu-oNC**), and nickel(II) (**Ni-oNC**) ions to furnish dinuclear complexes that were characterized by mix of mass spectrometry, NMR, EPR, electronic absorption spectroscopy, and for **Co-oNC**, single-crystal X-ray diffraction. Cofacial cobalt porphyrins are often active as catalysts for the Oxygen Reduction Reaction. Under heterogeneous conditions in water, **Co-oNC** was 83% selective for the electrocatalytic 4 e^-/4 H^+ reduction of O_2 to H_2O, matching homogeneous experiments which revealed consistent selectivity for H_2O (88%). This oNC core offers significant advantages over prisms formed by coordination-driven self-assembly: the dipyridnium-xylene coupling can furnish over 1 g of material in a single synthesis and the tethering motif is robust, maintaining a cofacial architecture in acidic and basic solutions. We envision this approach may be generalized to other bis-bromobenzyl building blocks, providing a means to tune metal−metal separation and other structural and electronic properties.

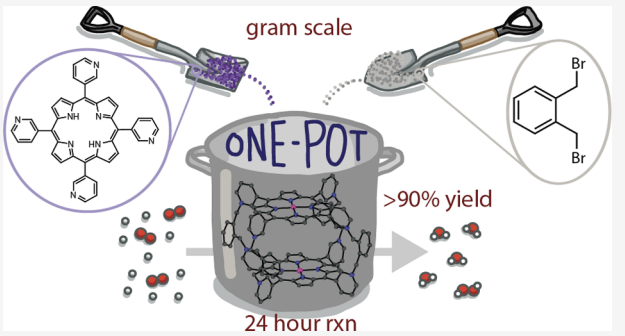

INTRODUCTION

Cofacial-porphyrinoid complexes have been widely used for a variety of applications including small molecule activation[1,2] and host−guest chemistry,[3−7] and therefore have been the center of research interest for decades.[8] The development of these materials is primarily motivated by their potential function, especially in mediating multielectron, multiproton chemistry; however, a recurring theme embedded within their study concerns the manner in which the macrocycles are structurally organized; in many cases their remarkable reactivity is matched by high synthetic complexity that can limit their practicality.

Over the past 50 years, several different approaches have been explored, with some key examples illustrated in Scheme 1. Early designs used stepwise, organic tethers using classic coupling motifs such as the amide bonds in the well-known FTF4 prism,[9] or carbon cross coupling as employed in the so-called Pacman porphyrins[8,10−13] (Scheme 1a,b). Although their multistep syntheses are low-yielding and require substantial chromatographic purification,[12,14,15] these designs are notable as being among the most selective molecular catalysts for the Oxygen Reduction Reaction (ORR), forming >95% H_2O. Their high performance yet challenging syntheses underpinned subsequent advances in this field seeking to maintain or enhance reactivity while introducing scalable and practical synthetic routes.

Along these lines, more recent designs have drawn upon noncovalent interactions to enforce a cofacial cleft. Highly active cofacial porphyrins held together by electrostatic interactions show a different option to orient multiple porphyrin faces and also provide the basis for rotaxane-tethers (Scheme 1c).[16] Over the past two decades, the use of metal−ligand bonding has been used to populate a wide library of cofacial designs wherein so-called molecular clips span pendant Lewis-basic donors decorating the macrocycles (Scheme 1d).[3,17−24] This coordination-driven self-assembly approach has been expanded beyond the cofacial motif to bring together three,[25,26] four,[27] and six porphyrins[28,29] into discrete molecular cages. The metal−ligand bonding approach is high-yielding and can be used to form highly active and selective catalysts, for example we have reported the formation of cofacial cobalt porphyrins at 82% yield that are 98%

Received: September 18, 2024
Revised: October 29, 2024
Accepted: November 5, 2024
Published: November 12, 2024

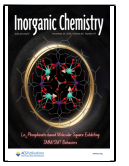

Scheme 1. Motifs to Enforce Cofacial Porphyrin Architectures Featuring (a) Amide Groups, (b) Rigid Aromatic Spacers Such as Anthracene and Dibenzofuran, (c) Rotoxane Tethers, (d) Dinuclear "Molecular Clips" That Form Metal-Pyridyl Bonds, and Alkylpyridinium Moieties Based on (e) Aryl-Pyridyl Spacers, and This Work, (f) Dipyridyl-Xylene Groups

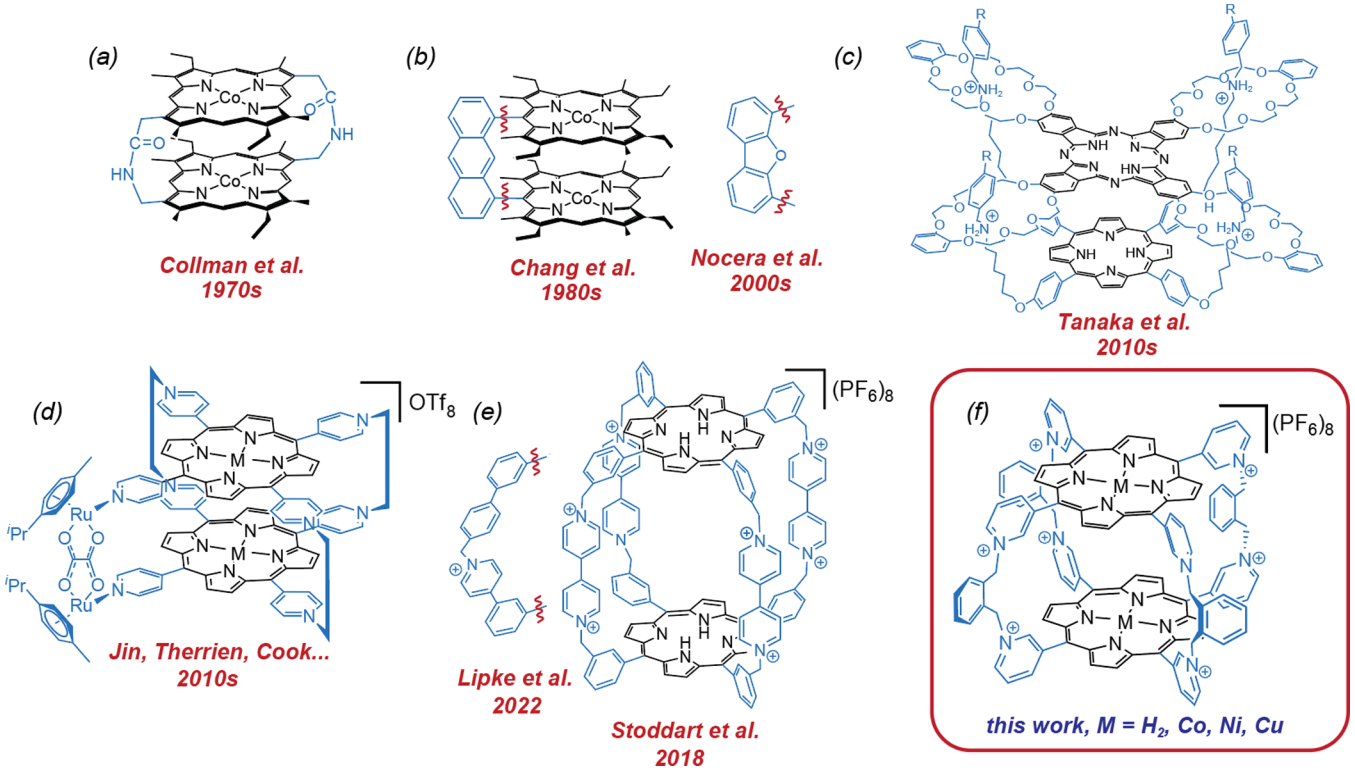

Scheme 2. Preparation of Free-base and Metalated oNCs from T3PyP and 1,2-Dibromoxylene

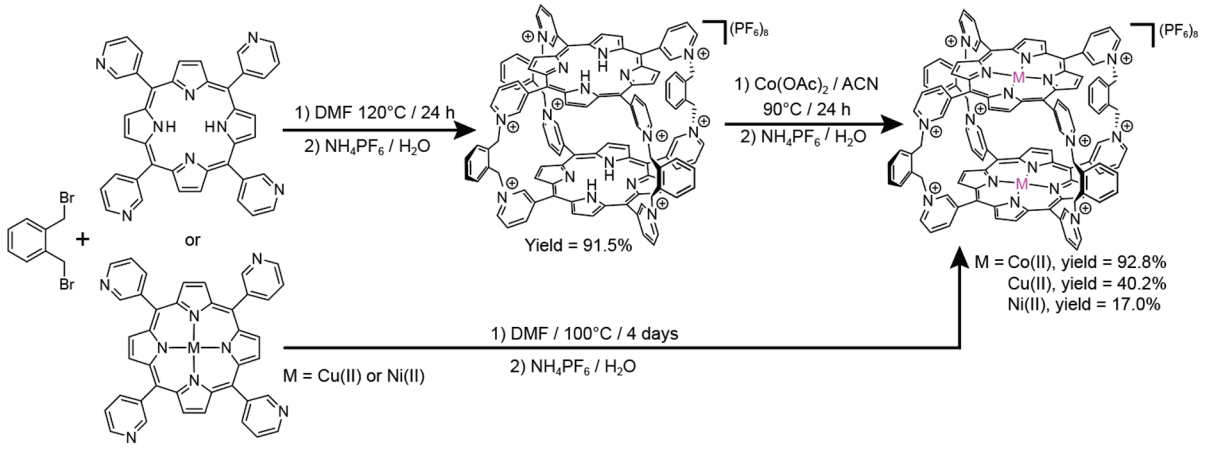

selective for water.[30] However, the use of precious metals in the molecular clips does limit the scalability and typical reactions have been limited to the 100 mg scope.[31,32]

To avoid metal ions that play a structural role, which can increase cost, introduce modes of decomposition at sensitive metal−ligand bonds, and obscure reactivity by introducing secondary sites that could participate in catalysis, recent work in the field has revisited organic coupling reactions. Contemporary designs have been inspired by molecular machinery and host/guest chemistry based on alkyl-pyridinium moieties, most simply and elegantly demonstrated by Stoddart's Blue Box.[33,34] The combination of a pyridyl functionalized building block with a alkylbromide has grown beyond the formation of boxes to include a library of tetracationic squares, cages, and other frameworks.[35−40]

Alkyl-pyridinium groups are well suited for the formation of cofacial porphyrins as they are prepared under catalyst-free conditions, and the associated counterions can be tuned to enable solubility in either organic or aqueous conditions. Exploiting their expertise in designing molecular scaffolds using these moieties, Stoddart and co-workers tethered tetrabromo-tolylporphyrins though four 4,4′-bipyridine linkers (Scheme 1e).[40−42] The two-step synthesis involved the initial formation of four pyridinium groups on a single porphyrin, after which the second macrocycle was added, a strategy that required 4 days of reaction time to obtain complete prisms with a ∼16% yield. A similar approach was used to link two tetrapyridyl

https://doi.org/10.1021/acs.inorgchem.4c03958
Inorg. Chem. 2024, 63, 22532−22541

porphyrins through a para-dibromoxylene with a similar two-step approach and 15-day reaction time with a 14% yield for the coupling steps.

A significant advance to this approach was described by Lipke and co-workers using the same alkylpyridinium moiety. They linked two distinct porphyrins, one containing the pyridyl precursor and one containing the bromotolyl precursor (Scheme 1e).[41] This was an important addition to the field for four reasons: first, the reaction time was shortened to 6 days. Second, the reaction was one-pot. Third, the yield was significantly higher for the coupling step, 57% at small scale. Fourth, the synthesis could be carried out at the gram scale, albeit with a lower yield of 40%.

We found these architectures to be an exciting advance to the field, but both designs have metal−metal separations that are beyond the typical range expected for selective ORR (Scheme 1f). Herein, we have adapted the alkylpyridinium approach with three significant advances: first, our reaction time was shortened to 24 hours under mild conditions (120 vs 200 °C). Second, the reaction occurred with a 91.5% yield from commercially available inexpensive starting materials. The one-pot and gram-scalable nature of the approach was maintained in our system. The so-called organic nanocage (oNC) could be metalated prior to cofacial formation (Ni, Cu) or after the two porphyrins were linked (Co) (Scheme 2). Additionally, the free-base (metal-free) and nickel oNCs were made to be water-soluble so that they could be evaluated for stability under highly acidic and highly basic conditions. The oNC and its metal analogues were characterized using NMR, EPR, crystallography, UV−vis, and mass spectrometry. Electrocatalytic studies were performed to evaluate the new cobalt cofacial porphyrin cage. This work establishes the development of a simply and quickly synthesized, large-scale, high-yielding new nanocage that is accessible as a scaffold for various applications.

EXPERIMENTAL SECTION

Materials. Chemicals were purchased from commercial sources and used as received unless otherwise noted. Solvents were purified using a solvent-drying system (Pure Process Technology). ^{1}H NMR spectra were acquired on a Varian INOVA 500 MHz spectrometer. Chemical shifts (δ) are reported in parts per million (ppm) and referenced against the residual proton resonances of the deuterated solvent. Mass spectra were recorded using the Agilent 6530 Q-TOF mass spectrometer. For the single-crystal X-ray diffraction, the sample was mounted on a MiTeGen loop and mounted on a Rigaku XtaLAB Synergy-S diffractometer equipped with PhotonJet-S Cu and Ag microfocus sources, and HyPix-6000HE hybrid pixel array detector. UV−vis spectra were acquired using a 1 cm quartz cuvette on an Agilent Technologies Cary 8454 UV−vis spectrophotometer. Electron paramagnetic resonance (EPR) data were acquired on a Bruker EMX spectrometer operating at 9.441 GHz.

Synthetic Procedures. *Synthesis of Free Base oNC.* 1,2-dibromoxylene (7.8 g, 30 mmol) was added to a solution of 5,10,15,20-tetra-3-pyridylporphyrin[43] (**T3PyP**) (927 mg, 1.5 mmol) in DMF (300 mL). After heating at 120 °C for 24 h, the mixture was cooled to room temperature and concentrated on a rotary evaporator under reduced pressure to ∼150 mL. The mixture was added to CH_2Cl_2, and the resulting precipitate was collected by filtration and washed with CH_2Cl_2 until the filtrate turned colorless (3 × 100 mL). The dark brown solid was stirred in water for two hours to dissolve the bulk of the material. Insoluble brown solids were removed by filtration. Excess NH_4PF_6 was added to the H_2O filtrate to precipitate a solid which was then filtered and washed with water (3 × 100 mL). The solid was allowed to dry on the filter paper overnight and then collected as a dark red solid (yield: 1.93 g, 91.5%). ^{1}H NMR (500 MHz, CD_3CN) δ 9.47 (d, J = 7.70 Hz, 8H pyridyl), 9.00 (d, J = 9.9 Hz, 8H pyridyl), 8.85 (s, 8H pyridyl), 8.48−8.68 (m, 24H pyrrolic, pyridyl), 7.79 (dd, J = 6.4 Hz, 4.9 Hz, 8H xylene phenyl), 7.47 (dd, J = 6.2 Hz, 4.3 Hz, 8H xylene phenyl), 6.33 (s, 16H xylene methylene), −4.40 (s, 4H pyrrolic NH). ESI-MS: m/z = 1261.747, corresponding to $[\text{cage} + 6PF_6^-]^{2+}$, m/z = 792.833, corresponding to $[\text{cage} + 5PF_6^-]^{3+}$ m/z = 558.452, corresponding to $[\text{cage} + 4PF_6^-]^{4+}$ m/z = 417.710, corresponding to $[\text{cage} + 3PF_6^-]^{5+}$. Soret band: λ_{max} = 416 nm, ε = 4.0 × 10^5 M^{-1} cm^{-1}, Q-band 1: λ_{max} = 511 nm, Q-band 2: λ_{max} = 543 nm, Q-band 3: λ_{max} = 585 nm, Q-band 4: λ_{max} = 642 nm.

Synthesis of Co-oNC. The metalation of the oNC with Co(II) was adapted from a related metalation of a porphyrin barrel.[26] A solution of **free base oNC** (90 mg, 0.032 mmol) in acetonitrile (∼10 mL) was stirred in a round-bottom flask, and a solution of $Co(OAc)_2{\cdot}4H_2O$ (64 mg, 0.26 mmol) in acetonitrile (∼10 mL) was then added to the reaction. The reaction mixture was brought to reflux for 24 h. The crude mixture was then cooled, and the solvent was removed under reduced pressure to ∼10 mL. The crude mixture was then added dropwise to an aqueous NH_4PF_6 solution (roughly 0.5 g NH_4PF_6 in 50 mL water). A red precipitate immediately formed. The red precipitate was filtered, washed with water (3 × 20 mL), allowed to dry on the filter paper overnight and collected as a dark red solid (yield: 87 mg, 92.8%). ESI-MS: m/z = 1318.705, corresponding to $[\text{cage} + 6PF_6^-]^{2+}$, m/z = 830.785, corresponding to $[\text{cage} + 5PF_6^-]^{3+}$ m/z = 586.847, corresponding to $[\text{cage} + 4PF_6^-]^{4+}$ m/z = 440.488, corresponding to $[\text{cage} + 3PF_6^-]^{5+}$. Soret band: λ_{max} = 429 nm, ε = 1.4 × 10^5 M^{-1} cm^{-1}, Q-band 1: λ_{max} = 537 nm. Crystallography: $P-1$ space group, a = 16.1044(6), b = 16.4655(8), c = 20.3076(8), α = 70.175(4), β = 88.160(3), γ = 82.179(4).

Synthesis of Cu-oNC. 1,2-dibromoxylene (2.6 g, 10 mmol) was added to a solution of copper(II) 5,10,15,20-tetra-3-pyridylporphyrin (**Cu T3PyP**) (340 mg, 0.5 mmol) in DMF (100 mL). After heating at 100 °C for 4 days, the mixture was cooled to room temperature and concentrated on a rotary evaporator under reduced pressure to ∼50 mL. The mixture was added to CH_2Cl_2, and the resulting precipitate was collected by filtration and washed with CH_2Cl_2 until the filtrate turned colorless (3 × 50 mL). The dark brown solid was stirred in water for two hours to dissolve the bulk of the material. Insoluble brown solids were removed by filtration. NH_4PF_6 was added to the H_2O filtrate and a brown solid immediately precipitates. Solid was filtered, washed with water (3 × 50 mL), allowed to dry on the filter paper overnight and then collected (yield: 295 mg, 40.2%). ESI-MS: m/z = 1323.157, corresponding to $[\text{cage} + 6PF_6^-]^{2+}$, m/z = 833.784, corresponding to $[\text{cage} + 5PF_6^-]^{3+}$ m/z = 589.187, corresponding to $[\text{cage} + 4PF_6^-]^{4+}$ m/z = 442.295, corresponding to $[\text{cage} + 3PF_6^-]^{5+}$. Soret band: λ_{max} = 414 nm, ε = 5.4 × 10^5 M^{-1} cm^{-1}, Q-band 1: λ_{max} = 540 nm, Q-band 2: λ_{max} = 575 nm. EPR: $g_\perp$ = 2.053, $g_\parallel$ = 2.203, $A_{Cu\perp}$ = −75 MHz, $A_{Cu\parallel}$ = −556 MHz.

Synthesis of Ni-oNC. 1,2-dibromoxylene (222 mg, 0.84 mmol) was added to a solution of nickel(II) 5,10,15,20- tetra-3-pyridylporphyrin (**Ni T3PyP**) (270 mg, 0.4 mmol) in dry DMF (80 mL). After heating at 100 °C for 4 days in a pressure vessel, the mixture was cooled to room temperature and concentrated on a rotary evaporator under reduced pressure to ∼50 mL. The mixture was added to CH_2Cl_2, and the resulting precipitate was collected by filtration and washed with CH_2Cl_2 until the filtrate turned colorless (3 × 50 mL). The dark brown solid was stirred in water for two hours to dissolve the bulk of the material. Insoluble brown solids were removed by filtration. NH_4PF_6 was added to the H_2O filtrate and a purple solid immediately precipitates. Solid was filtered, washed with water (3 × 50 mL), allowed to dry on the filter paper overnight and then collected (yield: 101 mg, 17%). ^{1}H NMR (500 MHz, CD_3CN) δ 9.44 (d, J = 5.0 Hz, 8H pyridyl), 8.93 (d, J = 5.0 Hz, 8H pyridyl), 8.80 (s, 16H pyrrolic), 8.73 (s, 8H pyridyl), 8.54 (t, J = 5.0 Hz, 8H pyridyl), 7.75 (dd, J = 10.0 Hz, 2.0 Hz, 8H xylene phenyl), 7.41 (dd, J = 10.0 Hz, 2.0 Hz, 8H xylene phenyl) 6.28 (s, 16H xylene methylene). ESI-MS: m/z = 1318.158, corresponding to $[\text{cage} + 6PF_6^-]^{2+}$, m/z = 830.452, corresponding to $[\text{cage} + 5PF_6^-]^{3+}$ m/z = 586.501, corresponding to $[\text{cage} + 4PF_6^-]^{4+}$ m/z = 440.290, corresponding to $[\text{cage} + 3PF_6^-]^{5+}$.

https://doi.org/10.1021/acs.inorgchem.4c03958
Inorg. Chem. 2024, 63, 22532−22541

Soret band: λ_{max} = 406 nm, $\varepsilon = 3.1 \times 10^5$ M^{-1} cm^{-1}, Q-band 1: λ_{max} = 524 nm, Q-band 2: λ_{max} = 558 nm.

Synthesis of Water-Soluble Free Base oNC-Br. Free base oNC (100 mg, 0.04 mmol) was added to ∼10 mL acetonitrile, and tetrabutyl ammonium bromide (∼100 mg, 0.31 mmol) was added to ∼10 mL acetonitrile and both solutions were allowed to solubilize. Once all solid was dissolved, the two solutions were mixed and a red-brown solid precipitated. The solution was left for 18 h and was subsequently centrifuged to collect the red solid (yield: 79.3 mg, 97.2%). ESI-MS: m/z = 1067.121, corresponding to $[\text{cage} + 6Br^-]^{2+}$, m/z = 684.421, corresponding to $[\text{cage} + 5Br^-]^{3+}$ m/z = 493.087, corresponding to $[\text{cage} + 4Br^-]^{4+}$.

Synthesis of Water-Soluble Ni-oNC-Br. **Ni-oNC** (44 mg, 0.015 mmol) was added to ∼10 mL acetonitrile, and tetrabutyl ammonium bromide (∼100 mg, 0.31 mmol) was added to ∼10 mL acetonitrile and both solutions were allowed to solubilize. Once all solid was dissolved, the two solutions were mixed and a red-brown solid precipitated. The solution was left for 18 h and was subsequently centrifuged to collect the red solid (yield: 25 mg, 70%). ESI-MS: m/z = 1123.051, corresponding to $[\text{cage} + 6Br^-]^{2+}$, m/z = 722.379, corresponding to $[\text{cage} + 5Br^-]^{3+}$ m/z = 522.051, corresponding to $[\text{cage} + 44Br^-]^{4+}$.

RESULTS AND DISCUSSION

Synthesis. The **free base oNC** was prepared by a S_N2 reaction between **T3PyP** and commercially available 1,2-dibromoxylene (Scheme 2). No precautions were taken to exclude air, water, or light throughout the synthesis in which all reagents were added at once. Reaction workup steps were done on the benchtop open to atmosphere. No column chromatography was used for purification resulting in facile and quick syntheses. The **Co-oNC** was metalated postsynthetically by treating formed **free base oNC** with a Co(II) source. In contrast, the **Cu-oNC** and **Ni-oNC** were synthesized by "pre-metalation," where **T3PyP** monomer was metalated, and then the metalated porphyrins were used to assemble the corresponding homodinuclear cages. The water-soluble oNC-Br cages were synthesized by carrying out an ion-exchange on the analogous nonwater-soluble cages. All six cages were characterized using small molecule techniques, each described in detail below.

NMR Analysis. The structure of the **free base oNC** in solution was initially probed by ^{1}H NMR and ^{13}C NMR spectroscopy, followed by two-dimensional (2D) NMR spectroscopy including COSY and ROESY. With the support of 2D techniques, all peaks in the ^{1}H NMR spectra were assigned unambiguously as shown in Figure 1. The peaks most useful in assigning structure were the xylene protons and the pyrrolic protons. The pyrrolic protons appear as a singlet (H_h), indicating that both positions are equivalent. The phenyl-based xylene peaks are doublets, where the protons at the 3,6 and 4,5 positions (denoted b and c in Figure 2) are equivalent. These equivalencies are most consistent with idealized D_{4h} symmetry, where the horizontal mirror plane and perpendicular C_2 axes relate these positions. Furthermore, this symmetry rules out monoporphyrin architectures or lower-symmetry oligomers, which are plausible given the excess 1,2-dibromoxylene used in the synthesis (20 equiv). If there was any twisting of the porphyrin faces, as seen in other cofacial porphyrin architectures, the pyrrolic peaks on the same five-member ring would no longer be equivalent and therefore they would couple with each other, resulting in a doublet.[30,44,45] DOSY experiments were also carried out to rule out the possibility of coordination polymer or oligomer formation. As seen in the DOSY spectra in Figure S7, all nonsolvent peaks share the same diffusion coefficient, consistent with all corresponding protons being on the same species. The diffusion coefficient was 4.33×10^{-10} m^2/s and the hydrodynamic radius was calculated as 14.4 Å, which is larger than the physical structure because the diffusion coefficient is influenced by ion paring and the solvation sphere.[46]

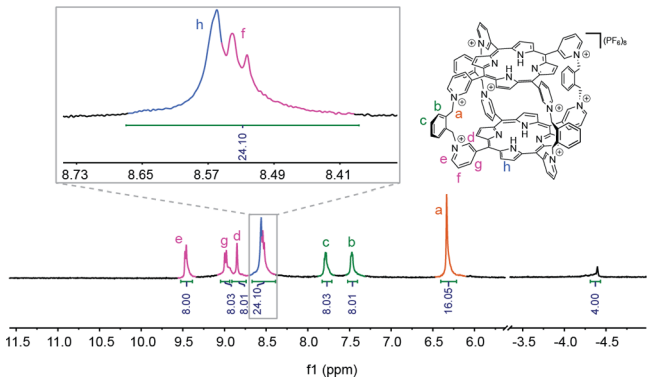

Figure 1. ^{1}H NMR (CD_3CN, 500 MHz) of **free base oNC**. Porphyrin signals are located in the region of 8.5−10.0 ppm, and the xylene signals are located in the region of 6.0−8.0 ppm. The signal at −4.4 is attributed to the pyrrolic NH peak.

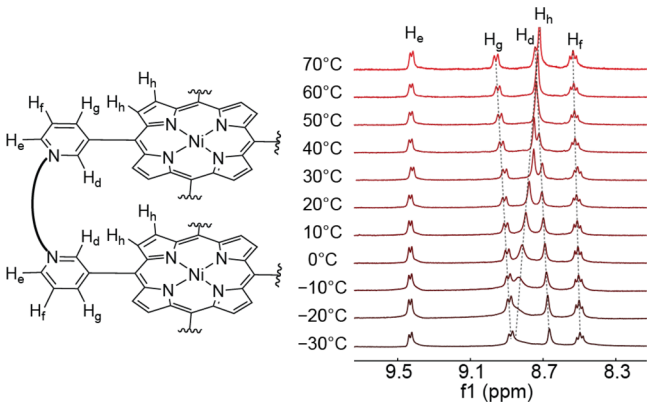

Figure 2. VT-NMR spectra of **Ni-oNC** (CD_3CN, 400 MHz). A simple illustration of the Ni-oNC structure (left), and the aromatic porphyrin region NMR spectra of the Ni-oNC from −30 to 70 °C.

Due to the paramagnetic nature of the cobalt and copper cages, the acquisition and analysis of their spectra would be challenging and offer limited information. Thus, a diamagnetic nickel analogue was more extensively characterized by NMR. The **Ni-oNC** NMR spectrum shows analogous peaks to that of its metal-free precursor, except for the NH peak at −4.40 ppm, a hallmark of free-base porphyrins. The DOSY NMR spectrum of the **Ni-oNC** is shown in Figure S8, with a single diffusion coefficient for all proton resonances belonging to the cage. The diffusion coefficient was measured as 5.17×10^{-10} m^2/s and the hydrodynamic radius of the **Ni-oNC** is 11.9 Å.

Variable-Temperature NMR (VT-NMR) experiments were conducted to further probe for structural information and the solution-state dynamics of these cages. The **Ni-oNC** was used for these experiments because it had sharper peaks relative to the **free base oNC**. The spectra were acquired over a temperature range of −30 to 70 °C (peaks associated with the porphyrin fragments shown in Figure 2). Across the temperature range, there were no obvious changes in the xylene signals that occur at 7.8, 7.5, and 6.4 ppm shown in Figures S11−S13. In the porphyrin region, some peak

https://doi.org/10.1021/acs.inorgchem.4c03958
Inorg. Chem. 2024, 63, 22532−22541

dynamics were observed. The meso pyridyl functional group, H_f, H_d, and H_g resonances shifted upfield. The pyrrolic CH proton H_h peak shifted downfield. These opposite shifts caused an overlap between H_g and H_h at −30 °C. As the sample warmed between 50 and 60 °C, an overlap was seen between H_d and H_h. Finally, at 70 °C H_d and H_h were separably resolvable once more. Notably, despite some shifts in the peaks, we observed no changes to splitting patterns for any of the protons that would be expected to occur during significant conformational changes which would alter the symmetry of the cage. For example, if the xylene spacer folded inward or flipped its orientation, the pyrrolic peaks would couple to one another. The observed dynamics may be due to changes in intermolecular forces resulting from different temperatures[47,48] or changes to the angles of the pyridyl rings or the breathing modes that alter the porphyrin-porphyrin distances, with no substantial folding or large conformation changes at the xylene spacers.

High-Resolution Mass Spectrometry. Mass spectrometry was used to verify the stoichiometry and the elemental composition of these supramolecular cages. As shown in Figure 3, the **free base oNC** contains a 2+ peak at 1261.747, a 3+ peak at 792.833, a 4+ peak at 558.452, and a 5+ peak at 417.710. These peaks correspond to intact cores (two free base **T3PyP** clipped with four xylene linkers) ionized by the loss of two, three, four, or five outer sphere hexafluorophosphate counterions, respectively.

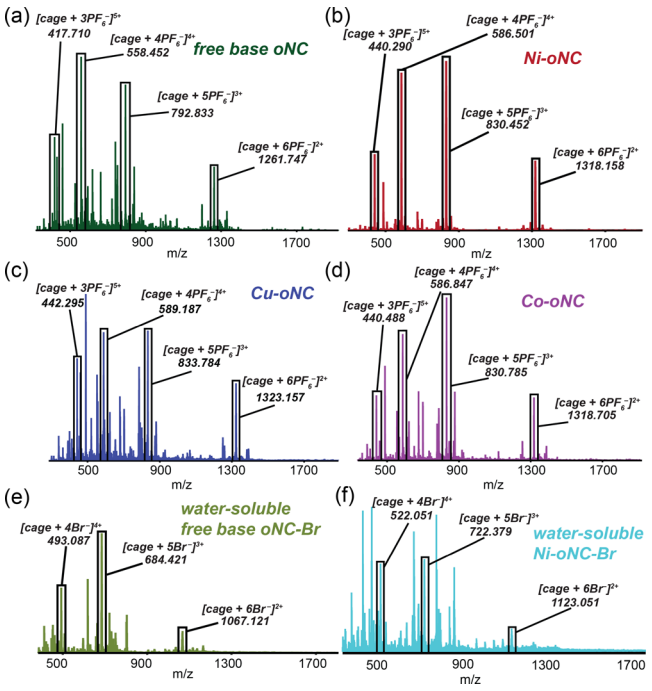

Figure 3. High-resolution mass spectrum of (a) **free base oNC**, (b) **Ni-oNC**, (c) **Cu-oNC**, (d) **Co-oNC** acquired in acetonitrile, (e) **water-soluble free base oNC-Br**, and (f) **water-soluble Ni-oNC-Br** acquired in water. In the full mass spectrum, labeled peaks correspond to the intact prism ionized by loss of outer sphere PF_6^- counterions for nonwater-soluble cages and Br^- for water-soluble cages.

The **Co-oNC** contains a 2+ peak at 1318.705, a 3+ peak at 830.785, a 4+ peak at 580.847, and a 5+ peak at 440.488, arising from intact cores (two cobalt **T3PyP** clipped with four xylene linkers) ionized by the loss of two, three, four, or five outer sphere hexafluorophosphate counterions, respectively. The presence of odd charge states, such as 3+ and 5+, particularly support our structural assignment of two-porphyrin, four-linker architectures. Species formed from half of these building blocks, such as bowtie-like structures that contain a single porphyrin and two linkers would not appear at these m/z values.

The **Cu-oNC** and **Ni-oNC** both contain four diagnostic peaks like the **free base oNC** and **Co-oNC**. For the water-soluble cages, the mass spectrograms were acquired from aqueous solutions, and the intact cores were ionized by the loss of outer sphere bromide ions. Taken together with the NMR data, our MS results strongly support the formation of four-strapped cofacial porphyrin cages.

Single-Crystal X-ray Diffraction. Single crystals of **Co-oNC** were grown from a DMF/diethyl ether mixture in the $P\bar{1}$ space group. Structure solution and refinement revealed the expected cofacial arrangement of the porphyrin units bridged by xylene moieties as seen in Figure 4. One-half formula unit comprises the asymmetric unit ($Z' = 0.5$) with the other half generated by the inversion symmetry operation ($Z = 1$). The xylene bridges are arranged such that the molecule possess C_{4h} point symmetry in the solid-state. The cobalt center is five coordinate; four nitrogen donors from the porphyrin and a partial occupancy aqua ligand (SOF refined to 0.91(2)) make up the primary coordination spheres of the Co(II) centers. The Co−Co distance was 7.566(3) Å. The eight cationic pyridinium groups were charge balanced by eight outer sphere PF_6^-. Four DMF molecules were well-resolved within the cavity between the two porphyrins. The folding inward of the xylene phenyl rings seen in the solid-state structure breaks the symmetry elements that make the pyrrolic protons equivalent, resulting in singlet peaks in the NMR. Since we do not observe coupling between the pyrrolic protons, we conclude that the crystal structure does not represent the solution-phase conformation. This is further supported by the methylene peaks of the xylene spacer, which also appear as a singlet in the NMR. In the solid-state structure, one methylene proton would be oriented toward a porphyrin face, and the other toward the internal cleft, breaking their equivalency.

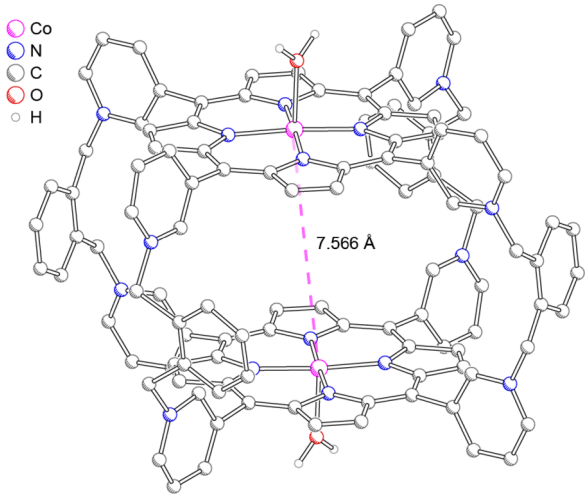

Figure 4. Ball-and-stick crystal structure of **Co-oNC**. Hydrogen atoms, outer-sphere PF_6^- ions, and cocrystallized DMF molecules have been omitted for clarity. Atoms color coded as follows: cobalt (magenta), oxygen (red), nitrogen (blue), and carbon (gray).

https://doi.org/10.1021/acs.inorgchem.4c03958
Inorg. Chem. 2024, 63, 22532−22541

Electron Paramagnetic Resonance. Further insight on electron and molecular structure were gleaned from electron paramagnetic resonance spectroscopy (EPR) of **Cu-oNC**. The EPR spectrum of **Cu-oNC** (Figure 5) shows a typical axial spin

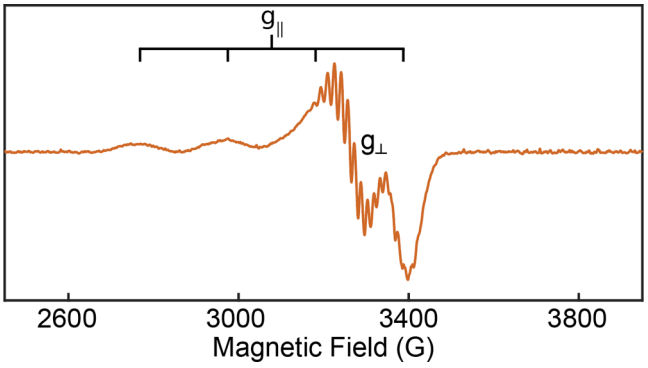

Figure 5. X-band EPR of **Cu-oNC** at 9.445 GHz frozen in a 25:75 DMF: toluene glass at 77 K.

system. The line shape is consistent with related mononuclear Cu(II), (d^9, $S = 1/2$) porphyrins. In a frozen glass the two Cu(II) centers are spatially separated enough to preclude dipolar interactions between the two unpaired electrons. No measurable half-field transition was observed; therefore, this system is likely best thought of as two isolated $S = 1/2$ spin systems molecularly tethered to each other and no metal−metal separation could be calculated from this data as has been used for other dicopper systems.[49,50] The lack of magnetic coupling agrees with the metal−metal separation predicted by the **Co-oNC** crystal structure as we do not expect any significant structural differences between the various metal-containing cages. The presumptive Cu−Cu separation of 7.566 Å would not be expected to result in coupling.[50] Clear $^{63}Cu/^{65}Cu$ hyperfine splitting was observed for the parallel transition. Further superhyperfine coupling of the unpaired electron to the ^{14}N nuclei of porphyrin ligand was observed superimposed on the perpendicular transition.

ORR Electrocatalysis. Dinuclear porphyrinoid complexes have been widely used as catalysts for a variety of small molecule activations[51] such as oxygen reduction reaction (ORR),[1,8,10,11,13,51−57] carbon dioxide reduction reaction (CO_2RR),[58−62] and hydrogen evolution reaction (HER).[11,63,64] While the multinuclearity of these species allow for multiproton/multielectron chemistry, there has been special emphasis placed on using dinuclear porphyrins for ORR. ORR catalyzed by metalated porphyrins or related complexes often proceed by one of two pathways: a four-proton/four-electron route to generate H_2O, or a two-proton/two-electron path to form H_2O_2.

To initially investigate the catalytic activity of the cobalt porphyrin complex, we conducted homogeneous cyclic voltammetry experiments. The cage was evaluated under four different conditions as seen in Figure 6a: blue (N_2, catalyst), red (O_2, catalyst), purple (N_2, trifluoroacetic acid (TFA), catalyst), and green (O_2, TFA, catalyst). Under N_2, there was no catalytic response. Under O_2, a reversible superoxide formation at the glassy carbon working electrode was observed with an $E_{1/2}$ value of −1.2 V versus FcH^+/FcH. With N_2 and TFA present as proton source, a catalytic wave was seen with an onset of −1 V vs FcH^+/FcH that we ascribe to the hydrogen evolution reaction (HER). Finally, under O_2

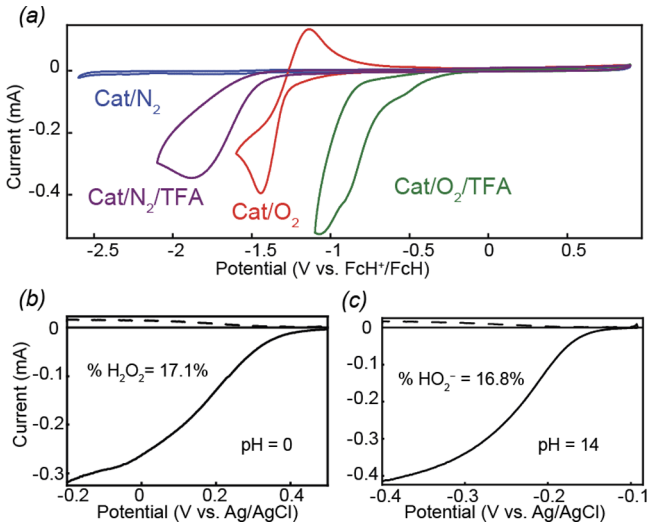

Figure 6. (a) Cyclic voltammograms of **Co-oNC** catalyst under homogeneous conditions. Blue: 0.1 mM **Co-oNC** (0.2 mM active cobalt porphyrin sites), N_2 atmosphere. Red: 0.1 mM **Co-oNC**, O_2 atmosphere. Purple: 0.1 mM **Co-oNC**, N_2 atmosphere, 100 mM TFA. Green: 0.1 mM **Co-oNC**, O_2 atmosphere, 100 mM TFA. In all cases, dry acetonitrile with 100 mM $TBAPF_6$ was used. Scan rate: 100 mV/s, scan direction: reduction first. (b) RRDE of **Co-oNC** with scan rate of 20 mV s^{-1} and 2500 rpm rotation rate at pH = 0, and at (c) pH = 14.

atmosphere with TFA present, an appreciable current response was observed with an onset far more positive than that for HER, which we attributed to the oxygen reduction reaction, consistent with other cofacial porphyrins we have studied.[30,32,44,49,65]

To further probe the ORR reactivity in the context of selectivity and kinetics, rotating disk electrode (RDE) studies were performed heterogeneously, wherein the catalysts were immobilized along with carbon black and Nafion on the surface of the glassy carbon electrode (GC). Voltammograms in 0.5 M H_2SO_4 and 1 M NaOH were collected under both N_2 and O_2 atmospheres using a three-electrode configuration. Under the potential window of interest, no background HER was observed, and all current response was attributed to ORR. Though these experiments were carried out heterogeneously, to further ensure that the cage stayed intact in these highly acidic and highly basic environments, **Ni-oNC-Br** was dissolved in aqueous solutions with various pH values and UV−vis spectra were recorded (Figure S35). The cage showed no indication of decomposition in conditions as acidic as pH = 0 (0.5 M H_2SO_4) and as basic as pH = 11 (1 mM KOH). The cage precipitated out of solution at pH ≥ 12, which we attributed to a counterion exchange from PF_6^- to OH^-.

Linear sweep voltammetry (LSV) was carried out with catalyst inks immobilized and rotated at various rates, as shown in Figures S51 and S52. Rotating ring disk electrode (RRDE) experiments were conducted in the same manner. In the RRDE experiment, H_2O_2 generated at the disk was oxidized at the ring. By comparing disk and ring current responses, the Faradaic efficiency (FE) was calculated. Figure 6b,c shows representative data and the values of these current responses that have been used for calculating the FE. The results are summarized in Table 1. For the **Co-oNC**, the selectivity improved to 17.1% H_2O_2 as compared to **Co TPyP** monomer (61.3%).[44] The **Co-oNC** selectivity is on par with that of our previously studied **Co_2Rhoxo** prism as well as other ruthenium

https://doi.org/10.1021/acs.inorgchem.4c03958
Inorg. Chem. 2024, 63, 22532−22541

Table 1. Parameters of Co(II) Catalyst Inks Determined by Electrochemical Analyses

catalyst	E_{onset} (V)	N_{app}	%H_2O_2 (%)	%H_2O (%)	k_s (M^{-1} s^{-1})
Co-oNC	0.25	3.7	17.1	82.9	1.5×10^{1}
Co_2 Rhoxo	0.39	3.7	14.5	85.5	2.3×10^{2}
Co TPyP	0.28	2.8	61.3	38.7	3.5×10^{0}
Co_2 Ag_4	0.40	2.7	65.5	34.5	5.0×10^{-1}

clipped Co_2 prisms under similarly acidic conditions.[30,44,66] In addition to the measurement of FE, we subjected our heterogeneous catalyst inks to Koutecký−Levich analyses to ultimately determine standard rate constants (k_s), which are summarized in Table 1. The standard rate constant is 1 order of magnitude greater than that of the monomeric **Co TPyP**. The k_s value of **Co-oNC** is lower than other Co_2 prisms, but far larger than the rigid **Co_2Ag_4** prism we previously reported.[65]

ORR Chemical Reduction. ORR reactivity can also be evaluated using chemical reductants as an electron source, a method first developed by Fukuzumi and Guilard.[67] In this method, ferrocene donates electrons, forming ferrocenium in situ. It is known that air-saturated benzonitrile has an O_2 concentration of 1.7×10^{-3} M.[8,67−69] For this experiment, a solution of air-saturated benzonitrile with 100 mM ferrocene, 15 mM $HClO_4$, and 25 μM cobalt catalyst (25 μM of **Co-oNC**, or 50 μM of **Co-MT3PyP**) was used. To avoid the continuous dissolution of O_2 into solution, a Teflon-lined screw-top cuvette was used. With the filled cuvette, dissolved oxygen could not be replenished into solution, enabling O_2-limited conditions. In the presence of the Co monomer and Co cage, the concentration of ferrocenium was tracked over several hours by monitoring the absorbance at 620 nm (Figure 7). The concentration of ferrocenium in solution was calculated using the measured absorbance and the molar absorptivity of ferrocenium, 330 M^{-1} cm^{-1}. Since the transformation of ferrocene to ferrocenium is a one-electron process, each molecule of ferrocenium in solution is equivalent to one electron used in ORR. If the reaction proceeded by only the 4 e^-/4 H^+ pathway, producing 100% H_2O, then the maximum concentration of ferrocenium in solution would be four times the limiting concentration of O_2, or 6.8 mM, shown as a dashed line in Figure 7. If the reaction proceeded by exclusively 2 e^-/2 H^+ pathway, forming 100% H_2O_2, then the maximum concentration of ferrocenium in solution would be two times the concentration of O_2 in solution, or 3.4 mM.[68] An observation of ferrocenium concentrations somewhere between 3.4 mM and 6.8 mM indicates a mixture of H_2O and H_2O_2 formation. To calculate the equivalents of electrons consumed (n), the maximum concentration of ferrocenium can be divided by the concentration of dissolved O_2, 1.7 mM. This value, n, somewhere between 2 and 4, can then be used to calculate the percent that each pathway is favored in the reaction.[68]

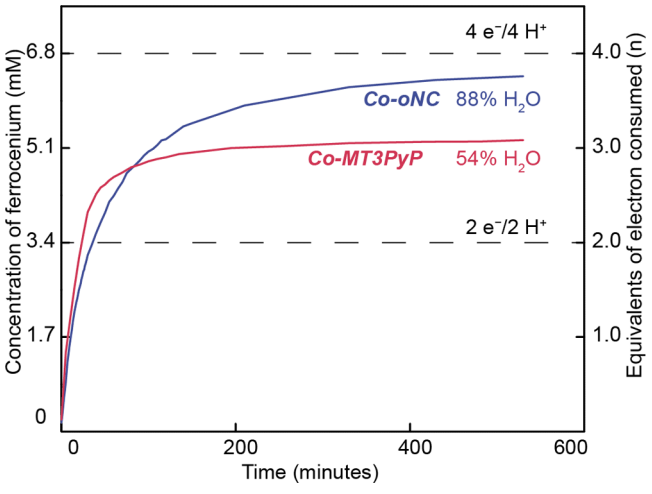

Figure 7. Chemical reduction ORR catalysis by monomeric cobalt catalyst (**Co-MT3PyP**, 0.05 mM), and dimeric cobalt catalyst (**Co-oNC**, 0.025 mM) monitored by ferrocenium formation (λ_{max} = 620 nm, ε = 330 M^{-1} cm^{-1}) in air-saturated PhCN (1.7×10^{-3} M) with 15 mM $HClO_4$ as proton source and 100 mM ferrocene initial concentration. The concentration of ferrocenium formation was plotted as a function of time. The number of electrons consumed and selectivity were calculated based on the concentration of ferrocenium formation during the reduction.

Under the O_2-limited conditions, **Co-oNC** showed fast kinetics and better selectivity for H_2O compared to the monomeric cobalt porphyrin. The selectivity of **Co-oNC** was 88% for the 4 e^-/4 H^+ pathway, as calculated from the plateau in ferrocenium, and is very similar to the selectivity determined electrochemically.

CONCLUSIONS

The use of alkylpyridinium bond formation as a structural element of molecular architectures has been recently adapted for the formation of cofacial porphyrins by Stoddard and Lipke. Here, we have expanded upon this approach, seeking to reduce the porphyrin-porphyrin separation using a short ortho-xylene spacer. In addition, we have enhanced aspects of the synthesis including the use of commercially inexpensive starting materials, mild and one-pot reaction conditions (120 °C, under air, in 24 h) with a reaction yield of 91.5% for the free-base cage. Dinuclear cobalt, copper, and nickel variants were made and characterized to determine stoichiometry, geometry, solid-state structure, and solution dynamics. Unlike our previous metal-clipped, self-assembled porphyrin prisms, the oNCs reported here adopt eclipsed rather than skewed porphyrin faces and appear to be rigid, as there is no evidence of significant conformational changes from VT-NMR studies. The cobalt analogue was evaluated for ORR catalysis both electrochemically and using a chemical reductant. In both methods, the **Co-oNC** favored the 4 e^-/4 H^+ reduction of O_2 to H_2O, (selectivity ~85%). The ability to synthesize cofacial porphyrin cages on a gram scale with ~24-h reaction time will greatly enhance the systematic study of these interesting architectures while also improving their practicality by reducing cost associated with precious metal clips, eliminating the possibility of clip-centered reactivity, and expanding the conditions (acidic, basic) in which they can be used.

ASSOCIATED CONTENT

Supporting Information

The Supporting Information is available free of charge at https://pubs.acs.org/doi/10.1021/acs.inorgchem.4c03958.

Synthesis procedures, ^{1}H NMR, ^{13}C NMR, 2D NMR, mass spectrometry, UV−vis, fluorescence, EPR, cyclic voltammograms, LSV, RRDE, and Koutecký-Levich analysis (PDF)

https://doi.org/10.1021/acs.inorgchem.4c03958
Inorg. Chem. 2024, 63, 22532−22541

Accession Codes

Deposition Number 2359150 contains the supplementary crystallographic data for this paper. These data can be obtained free of charge via the joint Cambridge Crystallographic Data Centre (CCDC) and Fachinformationszentrum Karlsruhe Access Structures service.

AUTHOR INFORMATION

Corresponding Author

Timothy R. Cook − *Department of Chemistry, University at Buffalo, The State University of New York, Buffalo, New York 14260, United States;* orcid.org/0000-0002-7668-8089; Email: trcook@buffalo.edu

Authors

Daoyang Zhang − *Department of Chemistry, University at Buffalo, The State University of New York, Buffalo, New York 14260, United States;* orcid.org/0000-0003-3722-1336

Rachel L. Snider − *Department of Chemistry, University at Buffalo, The State University of New York, Buffalo, New York 14260, United States;* orcid.org/0009-0002-5901-4442

Matthew R. Crawley − *Department of Chemistry, University at Buffalo, The State University of New York, Buffalo, New York 14260, United States;* orcid.org/0000-0002-2555-9543

Ming Fang − *Department of Chemistry, University at Buffalo, The State University of New York, Buffalo, New York 14260, United States;* orcid.org/0000-0002-1566-4825

Karla R. Sanchez-Lievanos − *Department of Chemistry, University at Buffalo, The State University of New York, Buffalo, New York 14260, United States*

Spencer Ang − *Department of Chemistry, University at Buffalo, The State University of New York, Buffalo, New York 14260, United States;* orcid.org/0009-0004-2809-4499

Complete contact information is available at: https://pubs.acs.org/10.1021/acs.inorgchem.4c03958

Author Contributions

D.Z.: conceptualization, experimental investigation, formal analysis, and writing−original draft. R.L.S.: experimental investigation, formal analysis, and writing−original draft. M.R.C.: crystal structure, EPR, formal analysis. M.F.: mass spectrometry investigation. K.R.S.-L.: crystal structure. S.A.: microwave synthesis training. T.R.C.: conceptualization, formal analysis, funding acquisition, project administration, supervision, validation, and writing−review and editing. D.Z. and R.L.S. contributed equally.

Funding

This work was supported by NSF CAREER Award 1847950 (TRC). Rigaku XtaLAB Synergy-S, a part of the Chemistry Instrument Center (CIC) at UB, was purchased with NSF CHE-2216151.

Notes

The authors declare no competing financial interest.

REFERENCES

(1) Chang, C. J.; Deng, Y.; Shi, C.; Chang, C. K.; Anson, F. C.; Nocera, D. G. Electrocatalytic four-electron reduction of oxygen to water by a highly flexible cofacial cobalt bisporphyrin. *Chem. Commun.* **2000**, 1355−1356.

(2) Rosenthal, J.; Luckett, T. D.; Hodgkiss, J. M.; Nocera, D. G. Photocatalytic Oxidation of Hydrocarbons by a Bis-iron(III)-μ-oxo Pacman Porphyrin Using O2 and Visible Light. *J. Am. Chem. Soc.* **2006**, *128*, 6546−6547.

(3) Nakamura, T.; Ube, H.; Shiro, M.; Shionoya, M. A Self-Assembled Multiporphyrin Cage Complex through Three Different Zinc(II) Center Formation under Well-Balanced Aqueous Conditions. *Angew. Chem., Int. Ed.* **2013**, *52*, 720−723.

(4) Sun, D.; Tham, F. S.; Reed, C. A.; Chaker, L.; Burgess, M.; Boyd, P. D. W. Porphyrin−Fullerene Host−Guest Chemistry. *J. Am. Chem. Soc.* **2000**, *122*, 10704−10705.

(5) Tashiro, K.; Aida, T. Metalloporphyrin hosts for supramolecular chemistry of fullerenes. *Chem. Soc. Rev.* **2007**, *36*, 189−197.

(6) Zhang, Z.; Ma, L.; Fang, F.; Hou, Y.; Lu, C.; Mu, C.; Zhang, Y.; Liu, H.; Gao, K.; Wang, M.; et al. Porphyrin-Based Multicomponent Metallacage: Host−Guest Complexation toward Photooxidation-Triggered Reversible Encapsulation and Release. *JACS Au* **2022**, *2*, 1479−1487.

(7) Kim, D.; Lee, S.; Gao, G.; Seok Kang, H.; Ko, J. A molecular-clip-based approach to cofacial zinc−porphyrin complexes. *J. Organomet. Chem.* **2010**, *695*, 111−119.

(8) Rosenthal, J.; Nocera, D. G. Role of Proton-Coupled Electron Transfer in O−O Bond Activation. *Acc. Chem. Res.* **2007**, *40*, 543−553.

(9) Collman, J. P.; Denisevich, P.; Konai, Y.; Marrocco, M.; Koval, C.; Anson, F. C. Electrode catalysis of the four-electron reduction of oxygen to water by dicobalt face-to-face porphyrins. *J. Am. Chem. Soc.* **1980**, *102*, 6027−6036.

(10) Collman, J. P.; Wagenknecht, P. S.; Hutchison, J. E. Molecular Catalysts for Multielectron Redox Reactions of Small Molecules: The "Cofacial Metallodiporphyrin" Approach. *Angew. Chem., Int. Ed. Engl.* **1994**, *33*, 1537−1554.

(11) Li, X.; Lei, H.; Xie, L.; Wang, N.; Zhang, W.; Cao, R. Metalloporphyrins as Catalytic Models for Studying Hydrogen and Oxygen Evolution and Oxygen Reduction Reactions. *Acc. Chem. Res.* **2022**, *55*, 878−892.

(12) Chang, C.; Abdalmuhdi, I. Anthracene pillared cofacial diporphyrin. *J. Org. Chem.* **1983**, *48*, 5388−5390.

(13) Chang, C. K.; Liu, H. Y.; Abdalmuhdi, I. Electroreduction of oxygen by pillared cobalt(II) cofacial diporphyrin catalysts. *J. Am. Chem. Soc.* **1984**, *106*, 2725−2726.

(14) Chang, C. J.; Baker, E. A.; Pistorio, B. J.; Deng, Y.; Loh, Z.-H.; Miller, S. E.; Carpenter, S. D.; Nocera, D. G. Structural, Spectroscopic, and Reactivity Comparison of Xanthene- and Dibenzofuran-Bridged Cofacial Bisporphyrins. *Inorg. Chem.* **2002**, *41*, 3102−3109.

(15) Deng, Y.; Chang, C. J.; Nocera, D. G. Direct Observation of the "Pac-Man" Effect from Dibenzofuran-Bridged Cofacial Bisporphyrins. *J. Am. Chem. Soc.* **2000**, *122*, 410−411.

(16) Mihara, N.; Yamada, Y.; Takaya, H.; Kitagawa, Y.; Aoyama, S.; Igawa, K.; Tomooka, K.; Tanaka, K. Oxygen Reduction to Water by a Cofacial Dimer of Iron(III)−Porphyrin and Iron(III)−Phthalocyanine Linked through a Highly Flexible Fourfold Rotaxane. *Chem. − Eur. J.* **2017**, *23*, 7508−7514.

(17) Lin, L.; Zhang, Y.-Y.; Lin, Y.-J.; Jin, G.-X. Half-sandwich rhodium and iridium metallamacrocycles constructed via C−H activation. *Dalton Trans.* **2016**, *45*, 7014−7021.

(18) Zhang, W.-Y.; Han, Y.-F.; Weng, L.-H.; Jin, G.-X. Synthesis, Characterization, and Properties of Half-Sandwich Iridium/Rhodium-Based Metallarectangles. *Organometallics* **2014**, *33*, 3091−3095.

(19) Han, Y.-F.; Lin, Y.-J.; Weng, L.-H.; Berke, H.; Jin, G.-X. Stepwise formation of "organometallic boxes" with half-sandwich Ir, Rh and Ru fragments. *Chem. Commun.* **2008**, 350−352.

(20) Gao, W.-X.; Zhang, H.-N.; Jin, G.-X. Supramolecular catalysis based on discrete heterometallic coordination-driven metallacycles and metallacages. *Coord. Chem. Rev.* **2019**, *386*, 69−84.

(21) Barry, N. P. E.; Govindaswamy, P.; Furrer, J.; Süss-Fink, G.; Therrien, B. Organometallic boxes built from 5,10,15,20-tetra(4-

pyridyl)porphyrin panels and hydroxyquinonato-bridged diruthenium clips. *Inorg. Chem. Commun.* **2008**, *11*, 1300−1303.
(22) Barry, N. P. E.; Austeri, M.; Lacour, J.; Therrien, B. Highly Efficient NMR Enantiodiscrimination of Chiral Octanuclear Metalla-Boxes in Polar Solvent. *Organometallics* **2009**, *28*, 4894−4897.
(23) Nakamura, T.; Ube, H.; Shionoya, M. Silver-Mediated Formation of a Cofacial Porphyrin Dimer with the Ability to Intercalate Aromatic Molecules. *Angew. Chem., Int. Ed.* **2013**, *52*, 12096−12100.
(24) Otsuki, J.; Sato, K.; Sugawa, K. A Cofacial Porphyrin Dimer Generated by Cooperative Zinc Ion Binding. *Eur. J. Inorg. Chem.* **2024**, *27*, No. e202400188.
(25) Blackburn, P. T.; Mansoor, I. F.; Dutton, K. G.; Tyryshkin, A. M.; Lipke, M. C. Accessing three oxidation states of cobalt in M6L3 nanoprisms with cobalt−porphyrin walls. *Chem. Commun.* **2021**, *57*, 11342−11345.
(26) Mansoor, I. F.; Dutton, K. G.; Rothschild, D. A.; Remsing, R. C.; Lipke, M. C. Uptake, Trapping, and Release of Organometallic Cations by Redox-Active Cationic Hosts. *J. Am. Chem. Soc.* **2021**, *143*, 16993−17003.
(27) Wood, D. M.; Meng, W.; Ronson, T. K.; Stefankiewicz, A. R.; Sanders, J. K. M.; Nitschke, J. R. Guest-Induced Transformation of a Porphyrin-Edged FeII4L6 Capsule into a CuIFeII2L4 Fullerene Receptor. *Angew. Chem., Int. Ed.* **2015**, *54*, 3988−3992.
(28) Meng, W.; Breiner, B.; Rissanen, K.; Thoburn, J. D.; Clegg, J. K.; Nitschke, J. R. A Self-Assembled M8L6 Cubic Cage that Selectively Encapsulates Large Aromatic Guests. *Angew. Chem., Int. Ed.* **2011**, *50*, 3479−3483.
(29) Zhang, D.; Ronson, T. K.; Nitschke, J. R. Functional Capsules via Subcomponent Self-Assembly. *Acc. Chem. Res.* **2018**, *51*, 2423−2436.
(30) Crawley, M. R.; Zhang, D.; Oldacre, A. N.; Beavers, C. M.; Friedman, A. E.; Cook, T. R. Tuning the Reactivity of Cofacial Porphyrin Prisms for Oxygen Reduction Using Modular Building Blocks. *J. Am. Chem. Soc.* **2021**, *143*, 1098−1106.
(31) Oldacre, A. N.; Friedman, A. E.; Cook, T. R. A Self-Assembled Cofacial Cobalt Porphyrin Prism for Oxygen Reduction Catalysis. *J. Am. Chem. Soc.* **2017**, *139*, 1424−1427.
(32) Zhang, D.; Rosch, L. E.; Crawley, M. R.; Cook, T. R. Post-synthetic modification of bis-iron(iii)-μ-oxo-porphyrin prisms to enhance oxygen reduction electrocatalysis. *Inorg. Chem. Front.* **2024**, *11*, 5557.
(33) Chen, X.-Y.; Chen, H.; Fraser Stoddart, J. The Story of the Little Blue Box: A Tribute to Siegfried Hünig. *Angew. Chem., Int. Ed.* **2023**, *62*, No. e202211387.
(34) Odell, B.; Reddington, M. V.; Slawin, A. M. Z.; Spencer, N.; Stoddart, J. F.; Williams, D. J. Cyclobis(paraquat-p-phenylene). A Tetracationic Multipurpose Receptor. *Angew. Chem., Int. Ed. Engl.* **1988**, *27*, 1547−1550.
(35) Barnes, J. C.; Juríček, M.; Vermeulen, N. A.; Dale, E. J.; Stoddart, J. F. Synthesis of ExnBox Cyclophanes. *J. Org. Chem.* **2013**, *78*, 11962−11969.
(36) Barnes, J. C.; Dale, E. J.; Prokofjevs, A.; Narayanan, A.; Gibbs-Hall, I. C.; Juríček, M.; Stern, C. L.; Sarjeant, A. A.; Botros, Y. Y.; Stupp, S. I.; et al. Semiconducting Single Crystals Comprising Segregated Arrays of Complexes of C60. *J. Am. Chem. Soc.* **2015**, *137*, 2392−2399.
(37) Frasconi, M.; Fernando, I. R.; Wu, Y.; Liu, Z.; Liu, W.-G.; Dyar, S. M.; Barin, G.; Wasielewski, M. R.; Goddard, W. A., III; Stoddart, J. F. Redox Control of the Binding Modes of an Organic Receptor. *J. Am. Chem. Soc.* **2015**, *137*, 11057−11068.
(38) Dale, E. J.; Vermeulen, N. A.; Juríček, M.; Barnes, J. C.; Young, R. M.; Wasielewski, M. R.; Stoddart, J. F. Supramolecular Explorations: Exhibiting the Extent of Extended Cationic Cyclophanes. *Acc. Chem. Res.* **2016**, *49*, 262−273.
(39) Roy, I.; Bobbala, S.; Zhou, J.; Nguyen, M. T.; Nalluri, S. K. M.; Wu, Y.; Ferris, D. P.; Scott, E. A.; Wasielewski, M. R.; Stoddart, J. F. ExTzBox: A Glowing Cyclophane for Live-Cell Imaging. *J. Am. Chem. Soc.* **2018**, *140*, 7206−7212.
(40) Chen, H.; Roy, I.; Myong, M. S.; Seale, J. S. W.; Cai, K.; Jiao, Y.; Liu, W.; Song, B.; Zhang, L.; Zhao, X.; et al. Triplet−Triplet Annihilation Upconversion in a Porphyrinic Molecular Container. *J. Am. Chem. Soc.* **2023**, *145*, 10061−10070.
(41) Rothschild, D. A.; Kopcha, W. P.; Tran, A.; Zhang, J.; Lipke, M. C. Gram-scale synthesis of a covalent nanocage that preserves the redox properties of encapsulated fullerenes. *Chem. Sci.* **2022**, *13*, 5325−5332.
(42) Shi, Y.; Cai, K.; Xiao, H.; Liu, Z.; Zhou, J.; Shen, D.; Qiu, Y.; Guo, Q.-H.; Stern, C.; Wasielewski, M. R.; et al. Selective Extraction of C70 by a Tetragonal Prismatic Porphyrin Cage. *J. Am. Chem. Soc.* **2018**, *140*, 13835−13842.
(43) Umezawa, N.; Matsumoto, N.; Iwama, S.; Kato, N.; Higuchi, T. Facile synthesis of peptide−porphyrin conjugates: Towards artificial catalase. *Bioorg. Med. Chem.* **2010**, *18*, 6340−6350.
(44) Zhang, D.; Crawley, M. R.; Oldacre, A. N.; Kyle, L. J.; MacMillan, S. N.; Cook, T. R. Lowering the Symmetry of Cofacial Porphyrin Prisms for Selective Oxygen Reduction Electrocatalysis. *Inorg. Chem.* **2023**, *62*, 1766−1775.
(45) Benavides, P. A.; Gordillo, M. A.; Yadav, A.; Joaqui-Joaqui, M. A.; Saha, S. Pt(ii)-coordinated tricomponent self-assemblies of tetrapyridyl porphyrin and dicarboxylate ligands: are they 3D prisms or 2D bow-ties? *Chem. Sci.* **2022**, *13*, 4070−4081.
(46) Evans, R.; Deng, Z.; Rogerson, A. K.; McLachlan, A. S.; Richards, J. J.; Nilsson, M.; Morris, G. A. Quantitative Interpretation of Diffusion-Ordered NMR Spectra: Can We Rationalize Small Molecule Diffusion Coefficients? *Angew. Chem., Int. Ed.* **2013**, *52*, 3199−3202.
(47) Gellman, S. H.; Dado, G. P.; Liang, G. B.; Adams, B. R. Conformation-directing effects of a single intramolecular amide-amide hydrogen bond: variable-temperature NMR and IR studies on a homologous diamide series. *J. Am. Chem. Soc.* **1991**, *113*, 1164−1173.
(48) Veroutis, E.; Merz, S.; Eichel, R. A.; Granwehr, J. Intra- and inter-molecular interactions in choline-based ionic liquids studied by 1D and 2D NMR. *J. Mol. Liq.* **2021**, *322*, No. 114934.
(49) Crawley, M. R.; Zhang, D.; Cook, T. R. Electrocatalytic production of hydrogen peroxide enabled by post-synthetic modification of a self-assembled porphyrin cube. *Inorg. Chem. Front.* **2022**, *10*, 316−324.
(50) Eaton, S. S.; Eaton, G. R.; Chang, C. K. Synthesis and geometry determination of cofacial diporphyrins. EPR spectroscopy of dicopper diporphyrins in frozen solution. *J. Am. Chem. Soc.* **1985**, *107*, 3177−3184.
(51) Xie, L.; Zhang, X.-P.; Zhao, B.; Li, P.; Qi, J.; Guo, X.; Wang, B.; Lei, H.; Zhang, W.; Apfel, U.-P.; et al. Enzyme-Inspired Iron Porphyrins for Improved Electrocatalytic Oxygen Reduction and Evolution Reactions. *Angew. Chem., Int. Ed.* **2021**, *60*, 7576−7581.
(52) Collman, J. P.; Marrocco, M.; Denisevich, P.; Koval, C.; Anson, F. C. Potent catalysis of the electroreduction of oxygen to water by dicobalt porphyrin dimers adsorbed on graphite electrodes. *Journal of Electroanalytical Chemistry and Interfacial Electrochemistry* **1979**, *101*, 117−122.
(53) Pegis, M. L.; Wise, C. F.; Martin, D. J.; Mayer, J. M. Oxygen Reduction by Homogeneous Molecular Catalysts and Electrocatalysts. *Chem. Rev.* **2018**, *118*, 2340−2391.
(54) Lv, B.; Li, X.; Guo, K.; Ma, J.; Wang, Y.; Lei, H.; Wang, F.; Jin, X.; Zhang, Q.; Zhang, W.; et al. Controlling Oxygen Reduction Selectivity through Steric Effects: Electrocatalytic Two-Electron and Four-Electron Oxygen Reduction with Cobalt Porphyrin Atropisomers. *Angew. Chem., Int. Ed.* **2021**, *60*, 12742−12746.
(55) Bhunia, S.; Ghatak, A.; Rana, A.; Dey, A. Amine Groups in the Second Sphere of Iron Porphyrins Allow for Higher and Selective 4e−/4H+ Oxygen Reduction Rates at Lower Overpotentials. *J. Am. Chem. Soc.* **2023**, *145*, 3812.
(56) Ghatak, A.; Bhunia, S.; Dey, A. Effect of Pendant Distal Residues on the Rate and Selectivity of Electrochemical Oxygen Reduction Reaction Catalyzed by Iron Porphyrin Complexes. *ACS Catal.* **2020**, *10*, 13136−13148.

https://doi.org/10.1021/acs.inorgchem.4c03958
Inorg. Chem. 2024, 63, 22532−22541

(57) Dey, S.; Mondal, B.; Chatterjee, S.; Rana, A.; Amanullah, S.; Dey, A. Molecular electrocatalysts for the oxygen reduction reaction. *Nat. Rev. Chem.* **2017**, *1*, No. 0098.
(58) Mohamed, E. A.; Zahran, Z. N.; Naruta, Y. Efficient electrocatalytic CO2 reduction with a molecular cofacial iron porphyrin dimer. *Chem. Commun.* **2015**, *51*, 16900−16903.
(59) Smith, P. T.; Benke, B. P.; Cao, Z.; Kim, Y.; Nichols, E. M.; Kim, K.; Chang, C. J. Iron Porphyrins Embedded into a Supramolecular Porous Organic Cage for Electrochemical CO2 Reduction in Water. *Angew. Chem., Int. Ed.* **2018**, *57*, 9684−9688.
(60) Guo, K.; Li, X.; Lei, H.; Guo, H.; Jin, X.; Zhang, X.-P.; Zhang, W.; Apfel, U.-P.; Cao, R. Role-Specialized Division of Labor in CO2 Reduction with Doubly-Functionalized Iron Porphyrin Atropisomers. *Angew. Chem., Int. Ed.* **2022**, *61*, No. e202209602.
(61) Guo, K.; Lei, H.; Li, X.; Zhang, Z.; Wang, Y.; Guo, H.; Zhang, W.; Cao, R. Alkali metal cation effects on electrocatalytic CO2 reduction with iron porphyrins. *Chinese Journal of Catalysis* **2021**, *42*, 1439−1444.
(62) Mondal, B.; Sen, P.; Rana, A.; Saha, D.; Das, P.; Dey, A. Reduction of CO2 to CO by an Iron Porphyrin Catalyst in the Presence of Oxygen. *ACS Catal.* **2019**, *9*, 3895−3899.
(63) Han, Y.; Fang, H.; Jing, H.; Sun, H.; Lei, H.; Lai, W.; Cao, R. Singly versus Doubly Reduced Nickel Porphyrins for Proton Reduction: Experimental and Theoretical Evidence for a Homolytic Hydrogen-Evolution Reaction. *Angew. Chem., Int. Ed.* **2016**, *55*, 5457−5462.
(64) Peng, X.; Zhang, M.; Qin, H.; Han, J.; Xu, Y.; Li, W.; Zhang, X.-P.; Zhang, W.; Apfel, U.-P.; Cao, R. Switching Electrocatalytic Hydrogen Evolution Pathways through Electronic Tuning of Copper Porphyrins. *Angew. Chem., Int. Ed.* **2024**, *63*, No. e202401074.
(65) Zhang, D.; Crawley, M. R.; Fang, M.; Kyle, L. J.; Cook, T. R. The rigidity of self-assembled cofacial porphyrins influences selectivity and kinetics of oxygen reduction electrocatalysis. *Dalton Trans.* **2022**, *51*, 18373−18377.
(66) Oldacre, A. N.; Crawley, M. R.; Friedman, A. E.; Cook, T. R. Tuning the Activity of Heterogeneous Cofacial Cobalt Porphyrins for Oxygen Reduction Electrocatalysis through Self-Assembly. *Chem. − Eur. J.* **2018**, *24*, 10984−10987.
(67) Fukuzumi, S.; Okamoto, K.; Gros, C. P.; Guilard, R. Mechanism of Four-Electron Reduction of Dioxygen to Water by Ferrocene Derivatives in the Presence of Perchloric Acid in Benzonitrile, Catalyzed by Cofacial Dicobalt Porphyrins. *J. Am. Chem. Soc.* **2004**, *126*, 10441−10449.
(68) Cai, Q.; Tran, L. K.; Qiu, T.; Eddy, J. W.; Pham, T.-N.; Yap, G. P. A.; Rosenthal, J. An Easily Prepared Monomeric Cobalt(II) Tetrapyrrole Complex That Efficiently Promotes the 4e−/4H+ Peractivation of O2 to Water. *Inorg. Chem.* **2022**, *61*, 5442−5451.
(69) Fukuzumi, S.; Imahori, H.; Yamada, H.; El-Khouly, M. E.; Fujitsuka, M.; Ito, O.; Guldi, D. M. Catalytic effects of dioxygen on intramolecular electron transfer in radical ion pairs of zinc porphyrin-linked fullerenes. *J. Am. Chem. Soc.* **2001**, *123*, 2571−2575.

https://doi.org/10.1021/acs.inorgchem.4c03958
Inorg. Chem. 2024, 63, 22532−22541